Trapping and Destruction of Long-Range High-Intensity Optical Filaments by Molecular Quantum Wakes in Air

S. Varma, Y.-H. Chen, and H. M. Milchberg

Institute for Research in Electronics and Applied Physics, University of Maryland, College Park, Maryland 20742, USA

We report the first observation of the strong effect of quantum rotational wave packets in atmospheric air on the long-range filamentary propagation of intense femtosecond laser pulses. In a pump-probe experiment, we find that the probe filament can be sucked into the pump filament's molecular quantum wake and trapped or be destroyed by it.

The propagation of few millijoule femtosecond laser pulses through gases routinely drives a large nonlinear response in the constituent atoms and molecules. This response is central to the extremely long-range filamentary propagation of ultrashort optical pulses in the atmosphere first demonstrated in 1995 [1] and since investigated by many groups [2]. Long-range filaments are accompanied by plasma generation and copropagating coherent white light generation. Femtosecond filaments are useful for several applications, including terahertz generation [3], remote ionization, nonlinear light generation and atmospheric monitoring [4,5], and channels for electrical discharges [6]. Shorter range filamentary propagation in closed gas cells has been applied to continuum generation [7], generation of high harmonics [8], and pulse compression [9]. Recently, several techniques have had success in controlling the formation of single filaments [10].

In this Letter, we demonstrate that the molecular alignment quantum wake following a pump pulse filamenting in air has a dramatic effect on the propagation of an intense probe pulse filament. For slight angular misalignment of pump and probe we find, depending on delay, that the rotational quantum wake either transversely pulls and focuses the probe filament into the pump filament path or destroys it. We also confirm that for pulse lengths >100 fs, the dominant air nonlinearity in single pulse filamentation is rotational. Accompanying probe pulse spectrum measurements are consistent with quantum wake trapping. Our results demonstrate that long-range filamentary propagation can be controlled by exploiting the coherent temporal and spatial response of air molecules.

As is well known [1,2], filament formation is the dramatic effect of the interplay between the third-order nonlinearity and ionization. The typical observed range for critical power in air for the self-focusing onset of filamentary propagation of femtosecond pulses is $P_{cr} = 3.77\lambda^2/8\pi n_0 n_2 \sim 5$–$10$ GW [1,2]. At sufficiently high self-focused intensity, multiphoton and field ionization of the gas atoms or molecules generates plasma along the beam axis. The free electrons form a negative lens that arrests self-focusing and causes refractive beam divergence. Self-focusing and arresting repeats when sufficient

nonlinear phase is again accumulated. In both simulations [11] and experiments [12] with air, this dynamic balancing has been observed to clamp the laser intensity at $\sim 5 \times 10^{13}$ W/cm^2 [2] and the gas ionization fraction at $\sim 10^{-4}$–10^{-3} [2,12]. The plasma filament is typically tens of microns in diameter [13] and can reach many meters in length.

For monatomic gases, the electronic nonlinearity embodied by n_2 is isotropic and nearly instantaneous. In air, however, the laser field-induced dipole moments in N$_2$ and O$_2$ are torqued toward alignment with the field [14]. This effect is significant in N$_2$ and O$_2$ ensembles at room temperature up to multiple atmospheres of pressure [7]. Quantum mechanically, the field-orientational effect is expressed as an excitation of a wave packet $|\psi\rangle = \sum_{j,m} a_{j,m}|j,m\rangle e^{-i\omega_j t}$ of rotational states $|j,m\rangle$ of energy $E_{j,m} = \hbar\omega_j = hcBj(j+1)$, where j and m are quantum numbers for rotational angular momentum and its component along the laser field, h is Planck's constant, and B is the rotational constant of the molecule [14]. The laser excitation leaves m for each molecule unchanged. Just as a short laser pulse results from the sum of phase-locked longitudinal modes of an optical cavity, this sum of rotational modes, phase-locked by the laser pulse, produces periodic, sharp molecular alignment recurrences. Owing to the even integer distribution $j(j+1)$ of the rotational frequencies, these recurrences occur dominantly at $1/4T$ intervals, where $T = 1/2Bc$ is the rotational period [15] ($T_{N2} = 8.3$ ps for nitrogen and $T_{O2} = 11.6$ ps for oxygen [16]). The transient refractive effect of these recurrences on a weak probe beam has been used as a diagnostic to measure them [7,16–18] or to induce spatial, phase, and spectral modulations [7,19,20].

Figure 1(a) shows the measured time and space alignment revivals induced by a 110 fs pump pulse in sealed gas cells of pure nitrogen and oxygen, using single-shot supercontinuum spectral interferometry [7]. The transient alignment is represented as $\langle\cos^2\theta\rangle_t - 1/3$, where θ is the angle between the laser polarization and the molecular axis and $\langle\rangle_t$ is the time-dependent ensemble average. For a pure molecular gas, the refractive index shift $\Delta n(r,t)$ owing to the alignment experienced by a parallel polarized probe

pulse is given by [7] $\Delta n(r, t) = 2\pi N n_0^{-1} \Delta\alpha(\langle\cos^2\theta\rangle_t - 1/3)$, where r is the coordinate transverse to the beam, N is the molecular density, $\Delta\alpha = \alpha_\parallel - \alpha_\perp$ (where $\alpha_\perp$ and $\alpha_\parallel$ are the linear polarizabilities along the short and long molecular axes, $\Delta\alpha_{N2} = 0.93 \times 10^{-24}$ cm³, and $\Delta\alpha_{O2} = 1.14 \times 10^{-24}$ cm³ [16]), and $n_0 \sim 1$ is the isotropic refractive index before the pump arrives. The effective alignment response of air, also shown in Fig. 1(a), is synthesized by forming $\langle\cos^2\theta\rangle_{t,\text{eff}} = 0.8(\Delta\alpha_{N2}/\Delta\alpha_{\text{eff}})\langle\cos^2\theta\rangle_{t,N2} + 0.2(\Delta\alpha_{O2}/\Delta\alpha_{\text{eff}})\langle\cos^2\theta\rangle_{t,O2}$, where $\Delta\alpha_{\text{eff}} = 0.8\Delta\alpha_{N2} + 0.2\Delta\alpha_{O2}$, using the approximate fractional abundances of N_2 and O_2 in air. In our experiments, we use a probe pulse polarized perpendicular to the pump; in that case $\langle\cos^2\theta\rangle_t$ is replaced by $(1 - \langle\cos^2\theta\rangle_t)/2$.

A central refractive index bump Δn will compete with beam diffraction for $\Delta n > (kz_0)^{-1}$, where k is the laser wave number and z_0 is the beam Rayleigh range. Therefore, a laser beam launched with f number $f_\# = \frac{1}{2} \times (\pi z_0/\lambda)^{1/2} > \frac{1}{2}(2\Delta n)^{-1/2} = f_{\#,\text{molec}}$ should be significantly affected by atmospheric molecular alignment revivals, where $f_{\#,\text{molec}}$ is the effective f number of the molecular index bump. For example, at the peak of the air quantum revival near $t = 8$ ps, which is comprised of the full revival of N_2 and the $3/4$ revival of O_2, $\langle\cos^2\theta\rangle_{t,\text{eff}} - 1/3 \sim 0.025$, giving $\Delta n(r = 0) \sim 3 \times 10^{-6}$
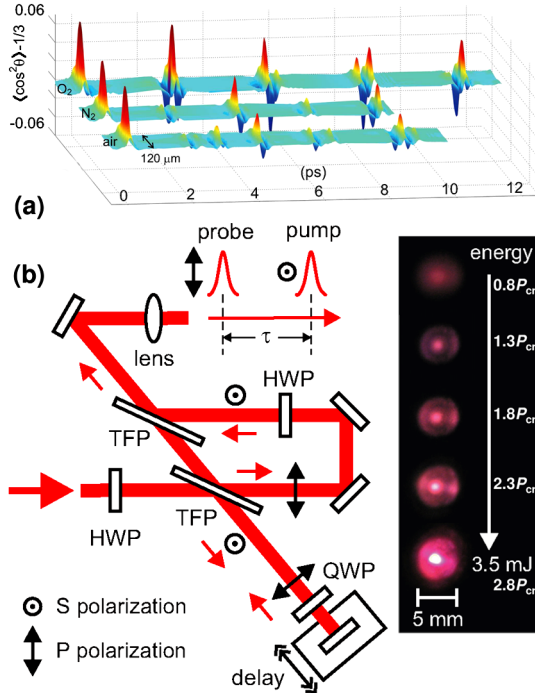

(a)

(b)

FIG. 1 (color online). (a) Measured alignment of 1 atm of N_2 and O_2 at room temperature (295 K) by a 110 fs, 800 nm, 4.1×10^{13} W/cm² laser pulse. The effective alignment of air is synthesized from the N_2 and O_2 plots (see text). (b) Setup showing the DPI. QWP = quarter wave plate; HWP = half wave plate; TFP = thin film polarizer. The right panel shows beam images of filamentation and white light generation for increasing pulse power up to $\sim 2.8 P_{\text{cr}}$.

at atmospheric pressure and giving $f_{\#,\text{molec}} \sim 200$. A molecular effect on propagation then requires $f_\# > 200$. The effect should also be substantial at any of the other revivals in Fig. 1(a).

The experimental setup is shown in Fig. 1(b). Orthogonally polarized, collinear pulses (pump and probe) are produced by a dual polarizer interferometer (DPI), with one arm delayed by a computer controlled stepper motor. For some experiments, the pump and probe directions were angularly separated. Few millijoule, 800 nm, 130 fs pulses of beam diameter 1 cm are focused by a 3 m lens at $f_{\#,\text{lens}} \sim 300$. The dual pulse beam propagates 6 m across the lab, reflects off two glass wedges, and is directed through a lens followed by a cube polarizer, filtering out the vertically polarized pump beam and allowing imaging of the probe on a CCD camera. Images are of a plane 25 cm after the filament, which is >2 m long. Also shown is a sequence of single beam images on a far-field screen, showing the onset of filamentation and white light generation up to $2.8 P_{\text{cr}}$ (using $P_{\text{cr}} = 10$ GW; see Fig. 2 caption).

An underappreciated aspect of rotational quantum wave packet excitation is its dominant ultrafast contribution to the air response for times near the pump pulse. For a wave packet which is a coherent sum of rotational states up to maximum rotational quantum number $j_{\max}$, the refractive index response time due to orientational effects alone is $\delta t \sim 2T/j_{\max}(j_{\max} + 1)$ [7]. For N_2 gas at room temperature, $j_{\max} \sim 20$ for $I_{\text{pump}} \sim 4 \times 10^{13}$ W/cm² [7], giving $\delta t \sim 40$ fs, a time scale confirmed by the inset in Fig. 2, a center lineout of the air response in Fig. 1(a). Unless a pulse is significantly shorter than ~ 40 fs, the nonlinear response of air is dominantly orientational, in contrast to earlier expectations [21]. As a demonstration of this strong effect, we generate a filament with the vertically polarized pump pulse (1.4 mJ, $1.1 P_{\text{cr}}$) and then follow it with the horizontally polarized probe (2 mJ, $1.5 P_{\text{cr}}$) for a range of delays near $t \sim 0$ (pump-probe overlap). Each pulse is sufficiently powerful to generate its own filament. Figure 2 shows a sequence of probe image slices taken at 30 fs intervals obtained by integrating the 2D CCD images along their vertical axis. Sample full images are shown at several delays. Well before $t = 0$, a strong probe pulse filament is seen as expected. Within approximately 50 fs of overlap, the probe filament is extinguished (location A in the figure) and remains so until ~ 50 fs beyond overlap, whereupon strong probe filamentation returns. The residual image at A is from polarizer leakage and side scattered probe light. The probe filament destruction is not caused by ionization defocusing induced by the pump filament plasma: The lifetime of the plasma is many nanoseconds [12], and the probe filament recovers on a femtosecond time scale. The destruction and recovery is caused by the neutral gas transient nonlinearity, dominated by the orientational contribution. As seen from Fig. 1(a) and the inset in Fig. 2, the peak air response near $t = 0$ will focus a probe polarized parallel to the pump. Here, our probe is
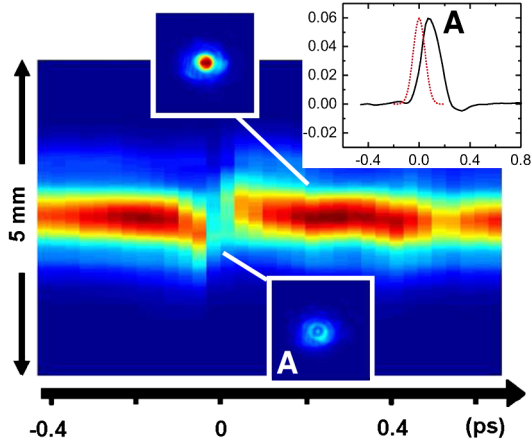
FIG. 2 (color online).   1D integrated images of probe filament as a function of delay (30 fs steps) through the pump-probe temporal overlap ($t = 0$). The laser pulse width is 130 fs. Pump/probe energies are 1.4 mJ/2 mJ ($1.1P_{cr}/1.6P_{cr}$). Each image slice is a 30-shot average. Selected 2D images are shown as insets, as is a beam center lineout of the air alignment response and the pump pulse (red squares) in the $t = 0$ region. Note that n_2 obtained from the inset gives $P_{cr} = 10$ GW at the laser pulse peak and $P_{cr} = 4.3$ GW at the molecular response peak.

perpendicularly polarized and must therefore *defocus*. The $\sim$100 fs filament disappearance interval is consistent with the molecular defocusing interval.

We now examine the effect of the later time wave packet revivals on probe filamentary propagation. Results near $t \sim$ 8 ps (sum effect of the full revival of N_2 and the 3/4 revival of O_2) are shown in Fig. 3(a) for pump/probe energies of 1.4 mJ ($1.1P_{cr}$)/2.5 mJ ($1.9P_{cr}$) and with pump and probe angularly separated by $\sim$0.1 mrad. Remarkably, during specific short intervals, the probe filament is seen not only to be extinguished but also *steered and enhanced*. From comparison with the $t \sim 8$ ps air revival lineout shown in the inset, we see that these intervals precisely map out the focusing and defocusing evolution of the molecular alignment. The filament destruction at locations A and B is coincident with the corresponding alignment peaks in the lineout. The strong steering and enhancement

coincide with the antialignment peaks at C and D. In these intervals, the probe filament is sucked into the pump filament's molecular quantum wake and trapped. After the revival, the probe filament returns to its original position. Full images of the filament at selected delays are shown as insets. On a shot by shot basis, and depending on pump-probe alignment, probe filament "destruction" is seen either as wild swings of the filament position or as beam breakup. The probe filament steering effect can be assessed by considering the required molecular Δn near the periphery of the pump filament in order that $k\Delta nL \sim 1$, where $L \sim 2$ m is the filament length. This gives $\Delta n \sim 6 \times 10^{-8}$, which is 0.002 of our measured Δn_{peak} value at $r = 0$. For 0.1 mrad pump-probe misalignment, the filaments are separated by $\sim$350 μm at their start. If the molecular lens profile corresponds to a Gaussian pump filament cross section with FWHM $\sim$100 μm, then $\Delta n/\Delta n_{peak} \sim 0.002$ for $r \sim 200$ μm, ensuring some spatial overlap of the probe filament with the pump-induced molecular lensing.

Figure 3(b) shows a sequence of fixed energy (4.4 mJ, $3.4P_{cr}$) probe delay scans near $t = 8$ ps for varying pump energy. Except at the lowest, subcritical, pump energy (0.85 mJ, $0.7P_{cr}$), the steering, enhancement, and extinguishing effects are all evident. The apparent robustness of the molecular effect over such a wide range of pump and probe powers is discussed below.

The effect on white light generation of probe injection into the trapping phase of quantum wakes is shown in Fig. 4(a). Panel (i) shows the single-shot images of the far-field pump ($2.3P_{cr}$) and probe ($2.5P_{cr}$) central filament spots offset by $\sim$0.1 mrad with the probe delay detuned from any revivals. Upon probe delay into location C of Fig. 3(a), it is steered and trapped by the pump filament, with a large increase in white light generation, shown in panel (ii), consistent with higher probe intensity and possible filament length extension. Delaying the probe to location A results in wild shot-to-shot probe expulsions from the pump filament, as captured in panel (iii).

While spectral and phase effects have been measured for weak probe pulses propagating though rotational wakes
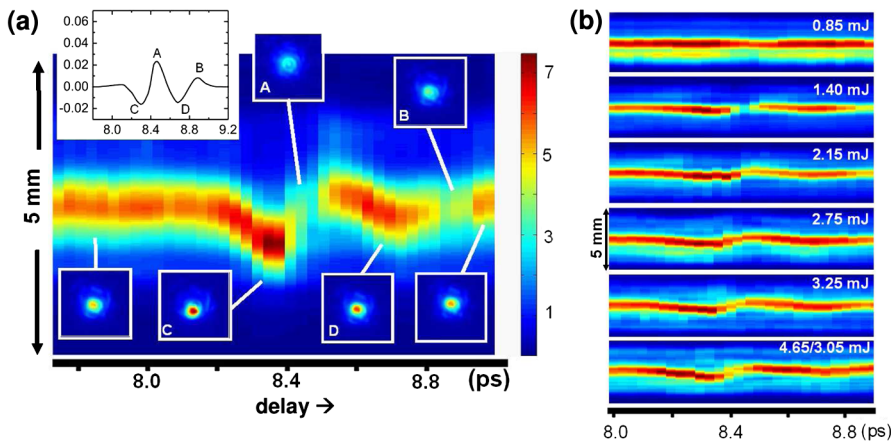

FIG. 3 (color online).   (a) 1D integrated images of probe filament as a function of delay (30 fs steps) through the air revival near $t = 8$ ps, comprised of the N_2 full revival ($t \sim T_{N2} \sim 8.3$ ps) and the O_2 three-quarter revival ($t = 3/4T_{O2} \sim 8.7$ ps). Pump/probe energies are 1.4 mJ/2.5 mJ ($1.1P_{cr}/2P_{cr}$). Selected 2D images are shown as insets, as is a lineout of the air alignment response in the $t = 8$ ps region. (b) Pump pulse energy scan ($0.7P_{cr}$ through $2.5P_{cr}$), holding probe energy constant at 4.35 mJ ($3.4P_{cr}$). The bottom panel has pump/probe energies 4.65 mJ/3.05 mJ ($3.6P_{cr}/2.4P_{cr}$).
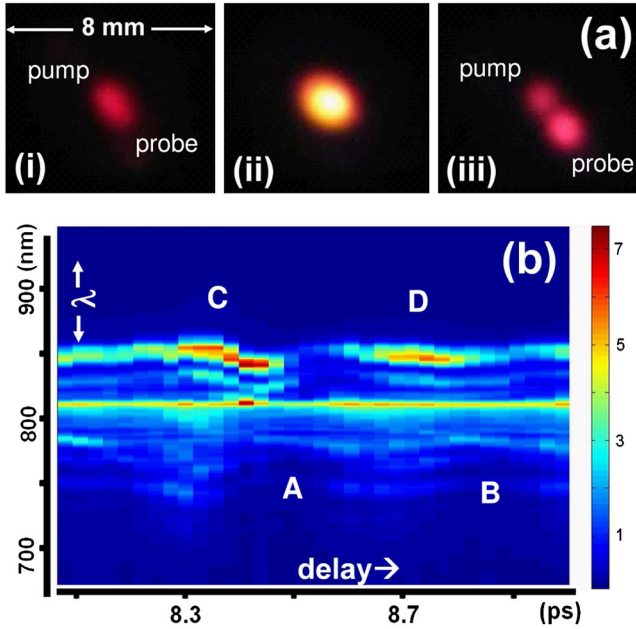
FIG. 4 (color online). (a) Pump $(2.3P_{cr})$ and probe $(2.5P_{cr})$ filament central spots in far field with initial ~ 0.1 mrad misalignment, where (i) the probe delay is detuned from revivals, (ii) the probe is delayed to location C in Fig. 3(a), and (iii) the probe is delayed to location A in Fig. 3(a). (b) Probe filament spectrum as a function of delay (30 fs steps) through the air alignment revival near $t = 8$ ps.

[7,18–20], an interesting question is the effect on the spectrum of a high power atmospheric filament propagating in an air molecular quantum wake. We measured probe filament spectra as a function of delay through the air revival at $t \sim 8$ ps by placing a spectrometer after the cube polarizer. A plot of probe filament spectrum in the ~ 800 nm region vs delay is shown in Fig. 4(b). The spectrum at each time slice is normalized by the spectrum integral over wavelength. A qualitative explanation of the spectrum is obtained from examining the inset of Fig. 3(a) and considering both linear and quadratic contributions to the phase modulation frequency shift: $\Delta\omega_{lin} \sim -\partial\Phi/\partial t$ and $\Delta\omega_{quad} \sim -(t-t_0)(\partial^2\Phi/\partial t^2)_{t=t_0}$, where $t = t_0$ is the peak of the local alignment. First, spectral reduction is consistent with locations A and B. Part of the broadened blue wing is consistent with molecular focusing leading to additional ionization at C and D, giving $\Delta\omega_{lin} > 0$ from ionization self-phase modulation. The molecular effect contributes both $\Delta\omega_{lin}$ and $\Delta\omega_{quad}$. $\Delta\omega_{lin}$ has both positive and negative contributions near the response inflection points. Additionally, the full probe pulse envelope experiences $\partial^2\Phi/\partial t^2 > 0$ in the focusing (C and D) intervals of the revival. This explains the redshift (for $t > t_0$) following the blueshift (for $t < t_0$) at C and D.

To complete the physical picture of the molecular effect on filament propagation, we must also consider plasma generation. The focusing effects are additive, so $f_{\#,molec} \sim 200$ and $f_{\#,lens} \sim 300$ combine to give $f_{\#,eff}^{-1} =$ $f_{\#,lens}^{-1} + f_{\#,molec}^{-1}$. Plasma-induced beam defocusing competes with molecular and lens focusing for $\frac{1}{2} \times (2\Delta n_{plasma})^{-1/2} > f_{\#,eff}$, where $\Delta n_{plasma} = N_e/2N_{cr}$, N_e is the electron density, and $N_{cr} \sim 1.7 \times 10^{21}$ cm^{-3} is the critical density at 800 nm. For $f_{\#,eff} \sim 120$, $N_e/N_{cr} < 1.7 \times 10^{-5}$. This is a fractional ionization of $<10^{-3}$ at atmospheric pressure, consistent with earlier measurements [2,12]. So even at the highest laser powers, essentially all molecules survive, explaining the robustness of the molecular effect.

In conclusion, we have established that molecular quantum wakes play a significant role in the propagation of high power femtosecond laser filaments in air. Wave packets of molecular rotational states not only dominate the prompt nonlinear response of air to femtosecond laser pulses of duration $> \sim 100$ fs, but the presence of their quantum echoes strongly controls the filamentation of properly timed intense trailing pulses. The molecular focusing effect is robust, surviving pump and probe pulses well beyond the critical power for filamentation, and may allow for a significant enhancement in filament length, continuity, and electron density. More complex pulse programming may enable fine control of long-range atmospheric propagation of high power lasers.

[1] A. Braun *et al.*, Opt. Lett. **20**, 73 (1995).
[2] For example, A. Couairon and A. Mysyrowicz, Phys. Rep. **441**, 47 (2007), and references therein.
[3] C. D'Amico *et al.*, Phys. Rev. Lett. **98**, 235002 (2007); Y. Liu *et al.*, Phys. Rev. Lett. **99**, 135002 (2007).
[4] I. Alexeev *et al.*, Opt. Lett. **30**, 1503 (2005).
[5] J. Kasparian *et al.*, Science **301**, 61 (2003).
[6] R. P. Fischer *et al.*, IEEE Trans. Plasma Sci. **35**, 1430 (2007); A. Houard *et al.*, Appl. Phys. Lett. **90**, 171501 (2007).
[7] Y.-H. Chen *et al.*, Opt. Express **15**, 11 341 (2007); **15**, 7458 (2007).
[8] H. R. Lange *et al.*, Phys. Rev. Lett. **81**, 1611 (1998); Y. Tamaki *et al.*, Phys. Rev. Lett. **82**, 1422 (1999).
[9] C. P. Hauri *et al.*, Appl. Phys. B **79**, 673 (2004).
[10] S. Eisenmann *et al.*, Opt. Express **15**, 2779 (2007); G. Fibich *et al.*, Opt. Express **14**, 4946 (2006).
[11] P. Sprangle *et al.*, Phys. Rev. E **66**, 046418 (2002).
[12] S. Eisenmann *et al.*, Phys. Rev. Lett. **98**, 155002 (2007).
[13] A. Ting *et al.*, Appl. Opt. **44**, 1474 (2005).
[14] H. Stapelfeldt and T. Seideman, Rev. Mod. Phys. **75**, 543 (2003).
[15] P. W. Dooley *et al.*, Phys. Rev. A **68**, 023406 (2003).
[16] C. H. Lin *et al.*, Phys. Rev. A **13**, 813 (1976).
[17] V. Renard *et al.*, Opt. Lett. **30**, 70 (2005).
[18] J.-F. Ripoche *et al.*, Opt. Commun. **135**, 310 (1997).
[19] R. A. Bartels *et al.*, Phys. Rev. Lett. **88**, 013903 (2002).
[20] F. Calegari *et al.*, Phys. Rev. Lett. **100**, 123006 (2008).
[21] E. T. J. Nibbering *et al.*, J. Opt. Soc. Am. B **14**, 650 (1997).